



Research article

Releasing of zinc ions from modified zinc oxide surfaces for improvement chemical crosslinks and antibacterial properties of acrylonitrile butadiene rubber films

Pornsiri Toh-ae¹, Raymond Lee-Nip², Yeampon Nakaramontri^{1*}

¹Sustainable Polymer & Innovative Composites Material Research Group, Department of Chemistry, Faculty of Science, King Mongkut's University of Technology Thonburi, Bangkok, Thailand

²Global Chemical Co., Ltd. Bangpoo Industrial Estate, Samutprakarn, Thailand

Received 3 April 2023; accepted in revised form 1 June 2023

Abstract. Acrylonitrile butadiene rubber (NBR) films filled with zinc oxide (ZnO) were prepared via latex mixing. The ZnO of commercial ZnO (ZnO_{WH}), ZnO nanoparticles (ZnO_{nap}), ZnO_{nap} -coated with calcium carbonate ($\text{ZnO}_{\text{nap-C}}$), and titanium dioxide ($\text{ZnO}_{\text{nap-T}}$) were investigated, and the mechanical and dynamic mechanical properties, crosslink density, and antibacterial activity of the resultant films were explored. The study found that the particle size and distribution of ZnO in the NBR films played a significant role in enhancing their properties. The incorporation of ZnO_{nap} resulted in a greater enhancement in the properties of the composite film than the ZnO_{WH} microparticles, with the greatest enhancement achieved with $\text{ZnO}_{\text{nap-C}}$. Furthermore, the composite films filled with 1 phr of $\text{ZnO}_{\text{nap-C}}$ exhibited 99.9% bacterial reduction efficacy against *Staphylococcus aureus* and *Escherichia coli* according to ISO 22196:2011 due to the release of reactive oxygen species and zinc ions across the rubber film layers to the bacterial surfaces. In addition, the bactericidal efficacy on the surface of the composite films was investigated by varying the contact kill times in accordance with ASTM D7907-14. The addition of $\text{ZnO}_{\text{nap-C}}$ at 4 phr reduced both bacterial levels by 92.00 and 51.85%, respectively, within 30 min. Hence, this research aims to contribute to developing new medical disinfection products, such as medical gloves and multipurpose rubber sheets.

Keywords: rubber, polymer composites, recycling, industrial application, material testing

1. Introduction

Acrylonitrile butadiene rubber (NBR), also known as nitrile rubber, is commonly synthesized through the copolymerization of acrylonitrile and butadiene monomers. This synthetic rubber is widely distinguished by its excellent heat stability, abrasion resistance, green strength, and oil resistance; thus, NBR is used in the production of several items, including disposable gloves, gaskets, oil seals, hoses, O-rings, automotive parts, footwear, etc. Notably, the need for NBR gloves has significantly increased since these present no allergenic concerns compared to commercial natural rubber (NR) gloves, though NBR has

lower elasticity [1]. However, as with other commercial rubber applications, NBR displays an inability to kill microorganisms on its surface. Hence, the incorporation of antibacterial agents into the rubber matrix has become necessary to inhibit the growth of microorganisms on the product surface. The bacteria *Staphylococcus aureus*, *Pseudomonas aeruginosa*, *Escherichia coli*, *Klebsiella pneumoniae*, *Serratia marcescens*, *Bacillus cereus*, *enterococci*, *Acinetobacter spp.*, and coagulase-negative staphylococci are frequently reported as causing hospital-associated infections. These microorganisms are responsible for human pathogenic diseases and cause

*Corresponding author, e-mail: yeampon.nak@kmutt.ac.th
© BME-PT

various infections, such as cholecystitis and cholangitis, peritonitis [2], nosocomial bloodstream infection [3], and respiratory and urinary infections [4]. Hospital-associated infections can be transmitted among people via exposure to contaminated water, food, and objects and physical contact with health-care workers [2]. Therefore, the development of products with microbial inhibitory properties has become a significant area of study.

Antibacterial agents are classified as organic and inorganic substances that can destroy or inhibit the growth of microorganisms by disrupting the bacterial membrane structure, resulting in the loss of cytoplasmic components [5]. The applications of inorganic antibacterial agents based on metal and metal oxide nanoparticles have frequently been investigated. Incorporating chemicals with smaller sizes and larger surface areas into the polymer matrix enhances the bacteria-killing efficiency of rubber films due to the resultant increased reactivity, unique quantum size effect, catalytic activity, and ability to release metal ions [6]. The majority of inorganic nanometals and nanometal oxides, including silver [7], copper [8], zinc oxide (ZnO) [9], titanium dioxide [10], *etc.*, have been intensively studied due to their antimicrobial behaviors.

Among these inorganic agents, ZnO constitutes a multifunctional species due to its unique physical and chemical properties, such as high thermal conductivity, a high refractive index, good photochemical activity, UV blocking, and antimicrobial activity together with easy incorporation into elastic polymers. ZnO is harmless to humans and is currently listed as generally recognized as safe (GRAS) by the United States Food and Drug Administration (FDA). Several mechanisms contribute to the antimicrobial activity of ZnO, including (i) the generation of reactive oxygen species (ROS), such as hydrogen peroxide, hydroxyl radicals ($\cdot\text{OH}$), and superoxide anion radicals ($\cdot\text{O}_2^-$); (ii) the release of Zn^{2+} ions; and (iii) electrostatic interactions that cause the oxidation of the bacterial cell membrane and cytoplasm [11]. In addition, ZnO nanoparticles are known to have an inhibitory effect on several pathogens, including Gram-positive and Gram-negative bacteria [12, 13], fungi [14], multiple drug-resistant (MDR) bacteria [15], and viruses [16].

However, ZnO is beneficial not only when used on its own but also when added to various manufactured materials in the plastic, fiber, glass, pigment, ceramic,

and rubber industries. In the last-mentioned industry in particular, ZnO is recognized as an activator in the vulcanization reaction in rubber matrices, which involves chemical crosslinking in unsaturated rubber molecules. In addition, the incorporation of ZnO into the polar NBR might contribute to electrostatic interactions, which lead to ionic crosslinking networks and enhanced mechanical properties [17]. In a study investigating the incorporation of ZnO in NR films via latex processes, modified ZnO, in particular, showed effective disruption of *E. coli* through the formation of ROS and Zn^{2+} ions, while less enhancement in the properties of the films was observed in the case of unmodified ZnO due to its low surface area and poor degree of dispersion [18]. This implies that the potential role of ZnO is mainly influenced by the degree of ZnO dispersion, the metric that determines the synergistic effect of the improvement in the mechanical and antibacterial properties of the rubber film. However, due to their specific surface areas, ZnO nanoparticles agglomerate easily, reducing the enhancement of the film properties. Thus, this necessitates the modification of ZnO for the dispersion of ZnO nanoparticles in the latex compound, related to increasing the effective surface area in the targeted object.

Therefore, this research aims to evaluate the incorporation of ZnO into NBR composite films by varying the ZnO loadings from 0–20 phr. Different types of ZnO were investigated, including white seal ZnO (ZnO_{WH}), ZnO nanoparticles (ZnO_{nap}), ZnO_{nap} -coated with CaCO_3 in a 90:10 $\text{ZnO}_{\text{nap}}:\text{CaCO}_3$ weight ratio ($\text{ZnO}_{\text{nap}}\text{-C}$), and ZnO_{nap} -coated with TiO_2 in a 50:50 $\text{ZnO}_{\text{nap}}:\text{TiO}_2$ weight ratio ($\text{ZnO}_{\text{nap}}\text{-T}$). The reinforcement of the NBR matrix with ZnO particles was evaluated based on its mechanical, crosslinking, and thermomechanical properties. The antibacterial activities of the NBR composite films were investigated using *Escherichia coli* (*E. coli*) and *Staphylococcus aureus* (*S. aureus*) as representatives of Gram-negative and Gram-positive bacteria, respectively. This research further aims to contribute to developing new medical disinfection products, such as gloves and multipurpose rubber sheets.

2. Experimental section

2.1. Materials

Acrylonitrile butadiene rubber (NBR) latex, with a solid content of 40% and containing 45% acrylonitrile content, was purchased from Norrawat Chemical

R1
R2
R3
R4
R5
R6
R7
R8
R9
R10
R11
R12
R13
R14
R15
R16
R17
R18
R19
R20
R21
R22
R23
R24
R25
R26
R27
R28
R29
R30
R31
R32
R33
R34
R35
R36
R37
R38
R39
R40
R41
R42
R43
R44

R45
R46
R47
R48
R49

Limited Partnership (Samut Sakhon, Thailand). The potassium hydroxide was manufactured by Qingdao Hisea Chem Co. Ltd., (Qingdao, China). In addition, 50% Sulfur, 50% zinc 2-mercaptobenzothiazole (ZMBT), and 50% Lowinox CPL (butylated reaction product of para-cresol and dicyclopentadiene) were purchased from Thanodom Trading Co., Ltd. (Bangkok, Thailand). Various types of ZnO particles used in this work are ZnO white seal grade (ZnO_{WH}) together with different types of ZnO nanoparticles (ZnO_{nap}), including ZnO_{nap}-adsorbed calcium carbonate (CaCO₃) at ZnO_{nap}:CaCO₃ ratios of 90:10% by weight (ZnO_{nap}-C) and ZnO-adsorbed titanium dioxide (TiO₂) at ZnO_{nap}:TiO₂ ratios of 50:50 by weight (ZnO_{nap}-T). All ZnO were supplied by Global Chemical Co., Ltd. (Samut Prakan, Thailand).

2.2. Preparation of NBR composite films

The NBR latex compound was carried out according to the formulation presented in Table 1. The latex compounding processes were initiated by the addition of potassium hydroxide solution, sulfur, ZMBT and CPL into NBR latex using a mechanical stirrer at 200 rpm. The mixing was continuously stirred at room temperature for 24 h to form a homogeneous latex compound. Then, the composite films were prepared by stirring the NBR latex compound for 3 min before filling ZnO and continued stirring for another 5 min. Afterward, the latex composite was poured directly into a glass plate and dried at 50 °C for 24 h in order to obtain the composite film at 0.1 mm of thickness slabs sheet.

3. Characterization

3.1. Molecular structure of ZnO

3.1.1. Particle size analyzer

The ZnO_{WH}, ZnO_{nap}, ZnO_{nap}-C and ZnO_{nap}-T were dispersed in the deionized water at 1.0 wt%. Particle

size and distribution of ZnO suspension were characterized using a light scattering particle size analyzer (HORIBA, LA600, Kyoto, Japan). The average particle size of materials was then reported.

3.1.2. Transmission electron microscope (TEM)

The morphologies of each ZnO particle were analyzed by a transmission electron microscope (TEM) (Model JEOL, JEM-1400, Tokyo, Japan) that operated with an acceleration voltage of 80 kV. The powder of specimens was dispersed in ethanol before sonicating for at least 30 min. The dispersion was finally dropped on the carbon-coated copper grid until the solvent evaporated completely, and the measurement was then started.

3.1.3. Inductively coupled plasma optical emission spectrometer (ICP-OES)

The qualification of Zn ions was analyzed by an inductively coupled plasma optical emission spectrometer (ICP-OES). The amount of total Zn ions in ZnO particles were prepared by the ZnO powder of 100 µg/ml dispersed in deionized water. The sample was incubated for 6 h before adding 0.5 ml of concentrated nitric acid. The solution was subjected to Zn analysis by an Inductively coupled plasma optical emission spectrometer (ICP-OES) (Optima 8000, Perkin Elmer, Massachusetts, USA). The dissolution of ZnO in an aqueous solution was also studied by filtering the ZnO suspension after incubation before analysis.

3.2. Properties of NBR/ZnO composite films

3.2.1. Tensile properties

Tensile properties of the NBR composite films were measured using a universal testing machine (Model 3365, Instron® Inc., Massachusetts, USA). The dumb-bell shape specimens were prepared according to ISO 37 type 2. The tests were performed at a cross-head speed of 500 mm/min.

3.2.2. Crosslink density

The crosslink densities of the composite film were performed using swelling in acetone. The sample with 10×10×0.1 mm was weight before immersing it into acetone at room temperature for 7 days according to the ASTM D471-79. The swollen samples were removed from the excess solvent before weighing the sample immediately and drying them in a hot air oven at 60 °C until the constant weight was reached.

Table 1. The formulation for the preparation of NBR composite foams filled with different types of ZnO.

Ingredients	Contents [phr]
40% NBR latex	100
10% Potassium hydroxide	1.0
50% Sulfur	2.0
50% ZMBT	1.0
25% ZnO _{WH}	0–20
25% ZnO _{nap}	
25% ZnO _{nap} -C	
25% ZnO _{nap} -T	

The crosslink density was calculated using the Flory-Rehner equation [19] (Equation (1)):

$$\nu = \frac{1}{V_s} \frac{\ln(1 - V_r) + V_r + \chi V_r^2}{V_r^{1/3} - \frac{V_r}{2}} \quad (1)$$

where ν is the crosslink density [mol/cm³], V_s is the molar volume of acetone, V_r is the volume fraction of rubber in a swollen network, χ is the Flory-Huggins interaction parameter between NBR and acetone, which is 0.351 [19].

3.2.3. Dynamic mechanical analysis (DMA)

Dynamic mechanical properties of the composite films were determined using a dynamic mechanical analyzer (Model DMA 1 STARe System, Mettler Toledo, USA). The samples were examined under the tension mode in the temperature region from –80 to 100 °C with a heating rate of 5 °C/min at a frequency of 10 Hz and a force of 0.2 N. The dynamic properties of storage modulus (E') and loss tangent ($\tan \delta$) were determined.

3.2.4. Morphologies

Morphological properties and energy dispersive X-ray analysis (EDX) of composites were characterized by scanning electron microscope (SEM) (Thermo Fisher Scientific, Massachusetts, USA) in order to see the dispersion of unmodified and modified ZnO inside the NBR matrix. Also, optical microscopy (OM) (Carl Zeiss Microscopy GmbH, Oberkochen, Germany) was applied to clarify the dispersion, distribution and roughness of the disinfectant films in a wide area.

3.2.5. Antibacterial properties

The antibacterial activity of the composite film was investigated against *Staphylococcus aureus* (*S. aureus*) (ATCC 6538P) and *Escherichia coli* (*E. coli*) (ATCC 8739) as representative of Gram-positive and -negative bacteria. The qualitative determination of antibacterial properties was performed by inhibition clear zone testing. The bactericidal efficiency on the film surface was determined according to ISO 22196:2011 and ASTM D7907-14.

In inhibition clear zone testing, A single colony of bacteria was incubated under the aseptic condition in Luria Broth (LB) medium (Becton, Dickinson and Company, New Jersey, USA) following incubation at 37 °C for 24 h in an incubator shaker (ES-60C, Hangzhou Miu Instruments Co., Ltd, Zhejiang,

China). Further, the bacterial concentrations in the suspensions were adjusted with LB to obtain turbidity of 0.5 McFarland (approximately 10⁸ CFU/ml) and spread onto the LB agar plate. The composite film with a diameter of 6 mm was sterilized with 70% ethanol (Ajax Chemical Co. Ltd., Samutprakarn, Thailand), then placed on the plate and incubated at 37 °C for 24 h. The antibacterial activity of the composite film was measured by the inhibition zone that was observed surrounding the sample [18].

The quantitative determination of the composite film surface was carried out according to ISO 22196:2011. The colony of bacteria was inoculated and cultivated at 37 °C for 24 h, and the bacterial suspension was adjusted with LB to obtain turbidity of 0.5 McFarland. The 400 µl of bacterial suspension was added onto the composite film surface (square pieces of 50×50 mm), then covered with 40×40 mm of sterilized polyethylene film to ensure even distribution of the bacterial suspension on the surface of the composite film. The sterilized Petri dishes containing the inoculated specimens were incubated at 35 °C for 24 h. After the incubation time, 10 ml of neutralizer was added to the Petri dish and shaken at 100 rpm. The bacterial suspension was collected and diluted using a ten-fold serial dilution method. The appropriate dilutions were then spread on an LB agar plate, which was incubated at 35 °C for 24 h. Bacterial colonies that appeared on the agar plates were counted and calculated as colony-forming units per ml [CFU/ml]. The results were reported as the percentage of bacterial reduction, as given in Equation (2):

$$\text{Reduction of bacteria [\%]} = \frac{A - B}{A} \quad (2)$$

where A and B are the average numbers of bacterial colonies containing samples without and with an antibacterial agent, respectively.

The standard testing for ASTM D7907 is the antimicrobial test method for the determination of bactericidal efficacy on the medical examination glove surface, which has contact kill times of 0, 5, 10, 20, and 30 min. The bacteria suspension was prepared with a turbidity of 0.5 McFarland. The 20 µl of bacteria solution was dropped onto the 10 cm² specimen surface and covered with sterilized polyethylene film. The inoculated specimens were incubated at 35 °C for 0, 5, 10, 20, and 30 min. After the specified time, the test specimen was transferred to a 50 ml

centrifuge tube that contained 10 ml of neutralizer solution. Then, the solution was vortexed for 15 seconds. Serial dilution of the neutralizer was performed. 100 μ l of each dilution was placed with the plate count agar and incubated at 35 °C for 24 h. The number of colonies in the petri dish agar was counted. The results were reported as the percentage of bacterial reduction, as given in Equation (2).

4. Results and discussion

4.1. Molecular structure of ZnO and modified ZnO

Physical appearance

Figure 1 depicts the molecular structures of the different types of ZnO particles, namely, ZnO_{WH}, ZnO_{nap}, ZnO_{nap}-C, and ZnO_{nap}-T. One can observe significant differences among the shapes of ZnO_{WH} and ZnO_{nap}.

Nanorods approximately 3 μ m in length are noted in ZnO_{WH}, while the spherical ZnO_{nap} exhibits a particle size of approximately 20 nm. Thus, the smaller particle size of the ZnO_{nap} might lead to a larger tendency for agglomeration than the other ZnO particles due to their large specific surface areas. However, in the case of their incorporation into rubber, this can provide the rationale for improving the crosslinking propagation and properties of the rubber composites. In the case of ZnO_{nap}-C and ZnO_{nap}-T, depicting the modification of ZnO_{nap} with CaCO₃ and TiO₂, respectively, one can observe the formation of smaller and looser ZnO_{nap} agglomerates. In addition, the larger size and higher concentration of the ZnO_{nap}-T particles indicate stronger agglomeration than in the case of ZnO_{nap}-C. The smaller size and lower concentration of ZnO_{nap}-C led to the better formation of

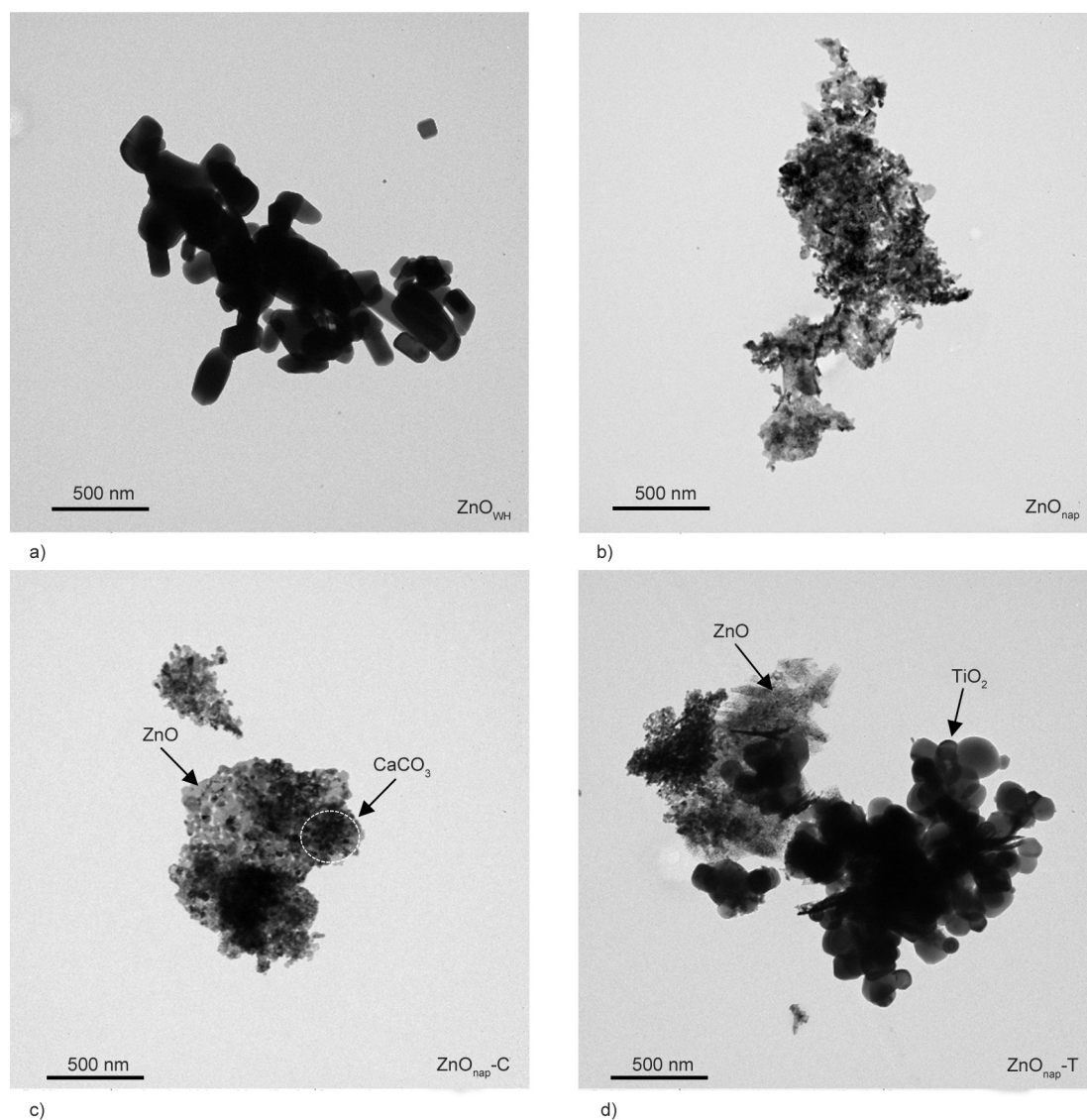


Figure 1. Physical morphologies of commercial ZnO_{WH} together with unmodified (a) and modified ZnO_{nap} shown in TEM images. a) ZnO_{WH}, b) ZnO_{nap}, c) ZnO_{nap}-C, d) ZnO_{nap}-T.

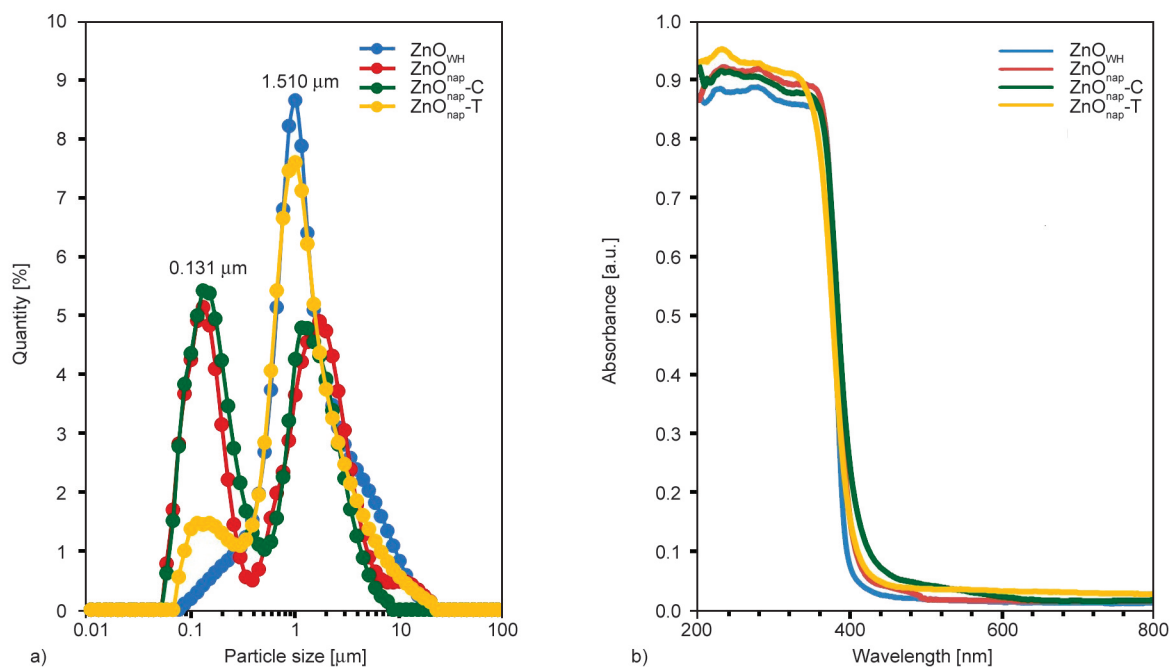


Figure 2. Particle size distribution from particle size analyzer (a) and UV-visible absorbance spectra (b) of commercial ZnO_{WH} together with unmodified and modified ZnO_{nap} .

the modified chemical. Furthermore, $\text{ZnO}_{\text{nap-C}}$ with a $\text{ZnO}_{\text{nap}}:\text{CaCO}_3$ ratio of 60:40 was also investigated in comparison to a 90:10 ratio, though the former yielded unsuitable properties. Therefore, suitable concentration ratios of ZnO_{nap} to CaCO_3 and TiO_2 were used in the present work.

In addition, corresponding to the TEM images in Figure 1, the particle sizes of the ZnO types, measured with a particle size analyzer, are indicated in Figure 2a. As expected, the ZnO_{nap} and $\text{ZnO}_{\text{nap-C}}$, using CaCO_3 to yield a modified core-shell filler, had the smallest particle sizes – approximately 0.1 μm – while the ZnO_{WH} and $\text{ZnO}_{\text{nap-T}}$ particles were approximately 1.5 μm in size. Further, Figure 2b depicts UV-visible absorbance spectra of the unmodified and modified ZnO particles to assess their absorption in the UV and visible regions. All four types of ZnO exhibit strong UV absorption in the range of 200–400 nm, and the ZnO_{WH} microparticles show lower absorption in the visible light region. Regarding the ZnO nanoparticles, $\text{ZnO}_{\text{nap-C}}$ exhibits a spectral shift toward the longer wavelength region, which induces electron movement after exposure to UV and visible light. This is a factor that affects the activation of the photocatalytic reaction for producing ROS on the rubber surface, which plays an important role in bacterial disruption.

ZnO particles are known to partially dissolve in aqueous solutions, releasing Zn^{2+} ions, which may

have an impact on antibacterial activity. The total and dissolved Zn^{2+} ion concentrations in aqueous solution were obtained from inductively coupled plasma optical emission spectroscopy (ICP-OES), as presented in Table 2. $\text{ZnO}_{\text{nap-T}}$ shows the lowest total Zn^{2+} ion concentration compared with the other ZnO types due to differences in the percentage of ZnO in the particles: $\text{ZnO}_{\text{nap-T}}$ consists of 50.2% ZnO, while ZnO_{WH} , ZnO_{nap} , and $\text{ZnO}_{\text{nap-C}}$ contain approximately 99.5, 97.8, and 91.4% ZnO, respectively. $\text{ZnO}_{\text{nap-C}}$ shows the highest concentration of dissolved Zn^{2+} ions, indicating that the modification of ZnO reduces the agglomeration of ZnO nanoparticles and enhances their dissolution. An increase in the Zn^{2+} concentration is principally responsible for enhanced zinc ion levels that activate chemical cross-linking and induce cytotoxicity in the disruption of bacterial cell membranes based on photocatalytic processes [20].

Table 2. Zinc ion contents of ZnO_{WH} together with unmodified and modified ZnO_{nap} received from coupled plasma optical emission spectroscopy (ICP-OES).

ZnO types	Zn ion contents [mg/l]	
	Total Zn	Soluble Zn
ZnO_{WH}	21.49 \pm 0.13	0.37 \pm 0.00
ZnO_{nap}	20.22 \pm 0.26	0.22 \pm 0.00
$\text{ZnO}_{\text{nap-C}}$	21.96 \pm 0.03	3.90 \pm 0.05
$\text{ZnO}_{\text{nap-T}}$	12.46 \pm 0.14	0.30 \pm 0.00

4.2. Properties of NBR/ZnO composite films

4.2.1. Mechanical properties

Figure 3 shows the stress–strain curves of the NBR composite films filled with different types and concentrations of ZnO, including the commercial ZnO (ZnO_{WH}) and the unmodified and modified ZnO_{nap} species. In addition, the mechanical properties, in terms of the moduli, tensile strength, and elongation at break, of each film are comparatively presented in Figure 4; sharp increases in the curves, particularly after 300% strain, are related to strain-induced crystallization (SIC) behavior, which is known to occur in NR [21]. Although NBR has a lower molecular weight and a shorter molecular main chain than NR, the existing $\text{C}\equiv\text{N}$ bonds in NBR lead to strong physical intermolecular forces among the NBR chains, especially during the stretching of the samples. Chemical crosslinking among NBR molecules relating to sulfur crosslinking processes also forms the rationale behind the restriction of the failure of NBR films during their stretching/extension in tensile testing. As expected, the degree of chemical crosslinking existing in the films strongly correlates to the activation reaction between the ZnO and the accelerator, which is the main chemical for propagating linkages between the main chains in the rubber. Thus, considering Figure 3, the stress–strain curves indicate two different SIC behaviors for ZnO loadings higher and lower than 2 phr. SIC is not

identified for 0, 0.5, and 1 phr of ZnO_{WH} , ZnO_{nap} , and $\text{ZnO}_{\text{nap-T}}$, which might be due to the poor dispersion of the ZnO species in the NBR matrix, leading to a lower potential for activating crosslinking within the film. With a low crosslink density, external forces can easily break the NBR films due to the films' low resistance to breakages. On the other hand, in the case of $\text{ZnO}_{\text{nap-C}}$, a strong increase in the stress–strain curve is indicated after extension up to at least 300% strain; this is due to the better dispersion ability of $\text{ZnO}_{\text{nap-C}}$, exhibiting better formation within the filler than $\text{ZnO}_{\text{nap-T}}$. Considering the NBR composite films with ZnO concentrations above 2 phr, strong SIC behavior can be observed for all the ZnO types. This implies that all the films display good resistance to breakage during extension at different optimal loadings within the NBR matrix. The results of the tensile properties obtained from the stress–strain curves are shown in Figure 4. Regarding the 100% modulus and tensile strength, greater efficiency in chemical crosslink propagation induces a strong increase in the modulus of the composite films. The modification of ZnO_{nap} with CaCO_3 effectively improves the dispersion and distribution of $\text{ZnO}_{\text{nap-C}}$ throughout the NBR matrix (Figures 4a and 4b). The activation of crosslinking is enhanced with the increasing degree of ZnO dispersion, with the optimal modulus achieved at approximately 10 phr for all ZnO types. Thus, the increase in the modulus

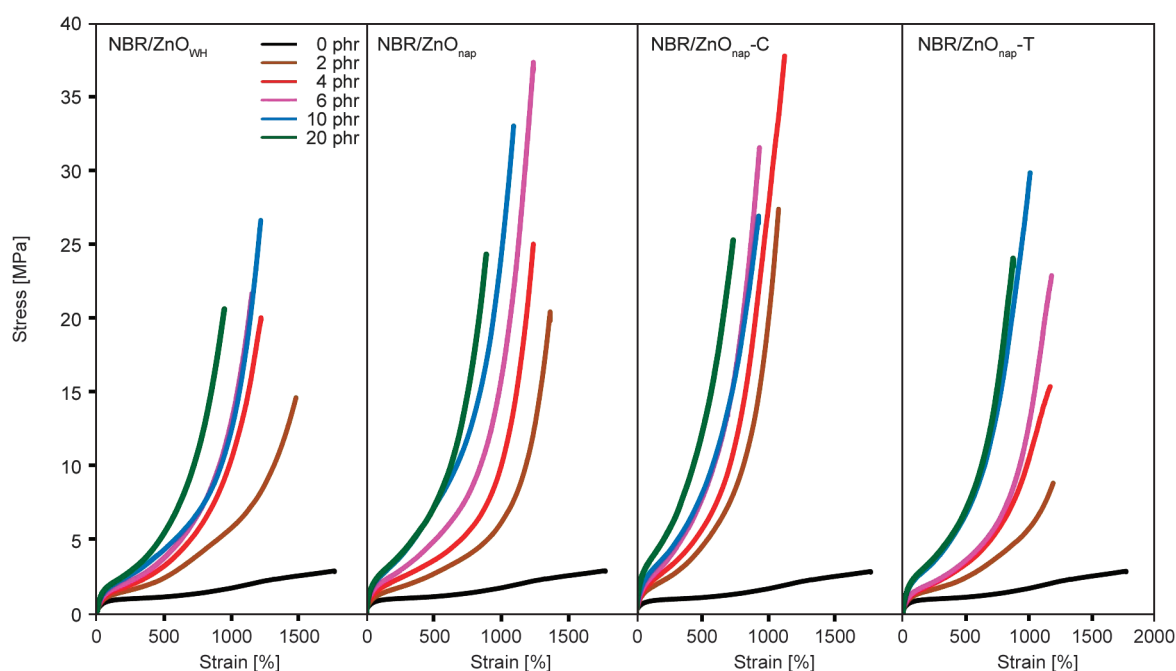


Figure 3. Stress-strain curves of NBR composite films filled with commercial ZnO_{WH} together with unmodified and modified ZnO_{nap} .

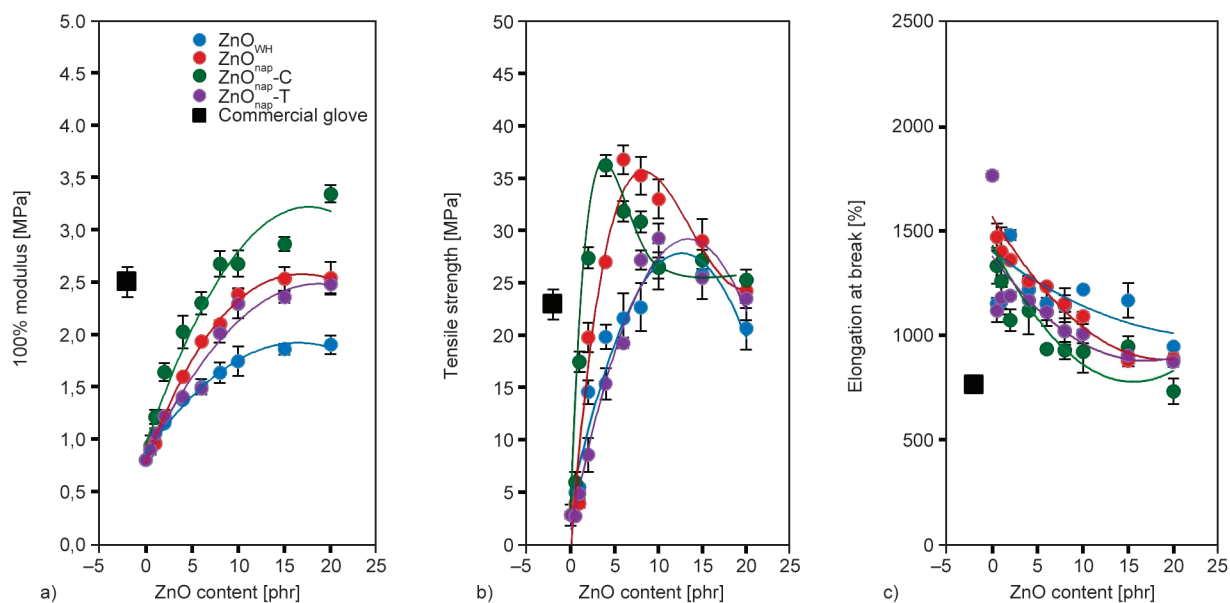


Figure 4. Tensile properties in terms of 100% moduli (a), tensile strengths (b) and elongation at breaks (c) of NBR composites films filled with commercial ZnO_{WH} together with unmodified and modified ZnO_{nap} .

leads to the composite films' resistance to failure. The optimal ZnO concentration for ZnO_{nap} and $\text{ZnO}_{\text{nap-C}}$ occurs at 4 phr before decreasing sharply with loadings above 4 phr. The unmodified ZnO_{nap} and $\text{ZnO}_{\text{nap-T}}$ show lower tensile strength at the same level as that of commercial NBR gloves, particularly in the range of 6–20 phr. However, the lowest elongation value of the NBR film filled with $\text{ZnO}_{\text{nap-C}}$ is still higher than that of commercial gloves; as expected, due to the film's strong resistance to failure, a larger force was applied, and, therefore, the film withstood breakage during stretching (Figure 4c). It should be noted that the commercial glove might utilize a different formulation and chemical concentration compared to the proposed composites.

Considering the activation of chemical crosslinking via the addition of ZnO_{WH} , ZnO_{nap} , and modified ZnO_{nap} , the chemical crosslink density (ν) was estimated based on the Flory–Rehner equation using the swelling method, as depicted in Figure 5. One can observe that ν has a good correlation with the obtained tensile properties of the NBR films. The optimal value of ν for ZnO_{WH} , ZnO_{nap} , and $\text{ZnO}_{\text{nap-T}}$ occurs at a loading of 4 phr, while the optimal concentration of $\text{ZnO}_{\text{nap-C}}$ for activating molecular chain crosslinking between the NBR molecules falls in the range from 4–10 phr. Considering the degree of crosslinking, one can note that the use of $\text{ZnO}_{\text{nap-C}}$ leads to a significantly higher ν value than the other ZnO types. It supports the hypothesis of the activation of the

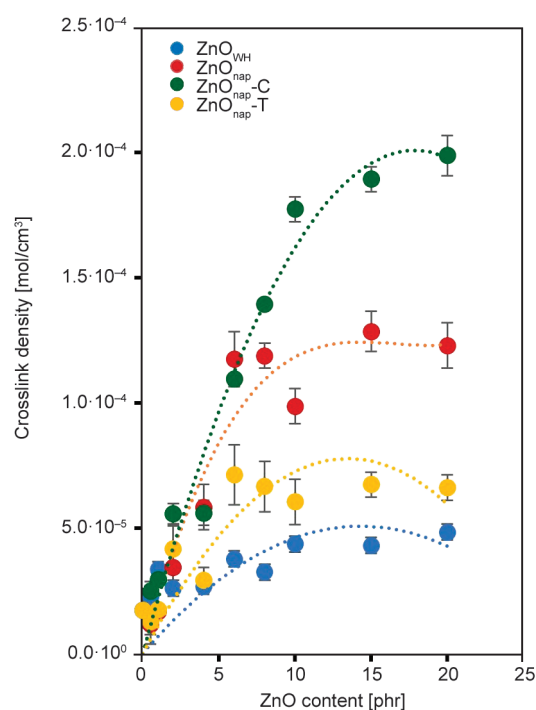


Figure 5. Crosslink density of NBR composites films filled with commercial ZnO_{WH} together with unmodified and modified ZnO_{nap} .

vulcanization reaction within the NBR matrix using CaCO_3 -coated ZnO_{nap} at the $\text{ZnO}_{\text{nap}}:\text{CaCO}_3$ wt% ratio of 90:10. One can conclude that the modification of ZnO_{nap} to $\text{ZnO}_{\text{nap-C}}$ leads to excellent performance in activating NBR crosslinking, which explains the improvement in the mechanical properties of NBR relating to the proper dispersion and distribution of $\text{ZnO}_{\text{nap-C}}$ throughout the NBR matrix. For

more details, Figure 6 displays the proposed chemical crosslinks among NBR molecules through sulfur curing using ZnO as the activator and filler. Step A, formations of ZnO and sulfur atoms together with the accelerated complex origination based on the reaction of ZnO and accelerator are initiated as seen in (A1) and (A2) of Figure 6, respectively [22]. At this step, reaction formation was activated by heating during chemical crosslinking propagation, so-called vulcanization processes, and therefore reaction efficiency depends on surface areas and degrees of dispersion of ZnO particles which can react to sulfur and also accelerator relating Zn ions releasing mechanism. In Step B, the chemical reaction to the NBR

chains had innovated, and the rubber-bound pendant groups were formed correlating the inserting $-S_x-O^*$ into the main rubber chains at the allylic carbon position in butadiene unit (B1) [22]. In parallel, the zinc-nitrile complex formation is fabricated among Zn ions and Zn compounds to the $-CN$ functional groups in the acrylonitrile unit (B2) of Figure 6 [23]. Zn ions play an important role in this step, and therefore, it was the reason for the high mechanical properties in NBR/ZnO_{nap}-C films since the ZnO_{nap}-C had strongly released Zn ions regarding finding in ICP-OES. Since the zinc-nitrile complex is concerned, the active sulphurating agent formed during the vulcanization reaction might be further involved

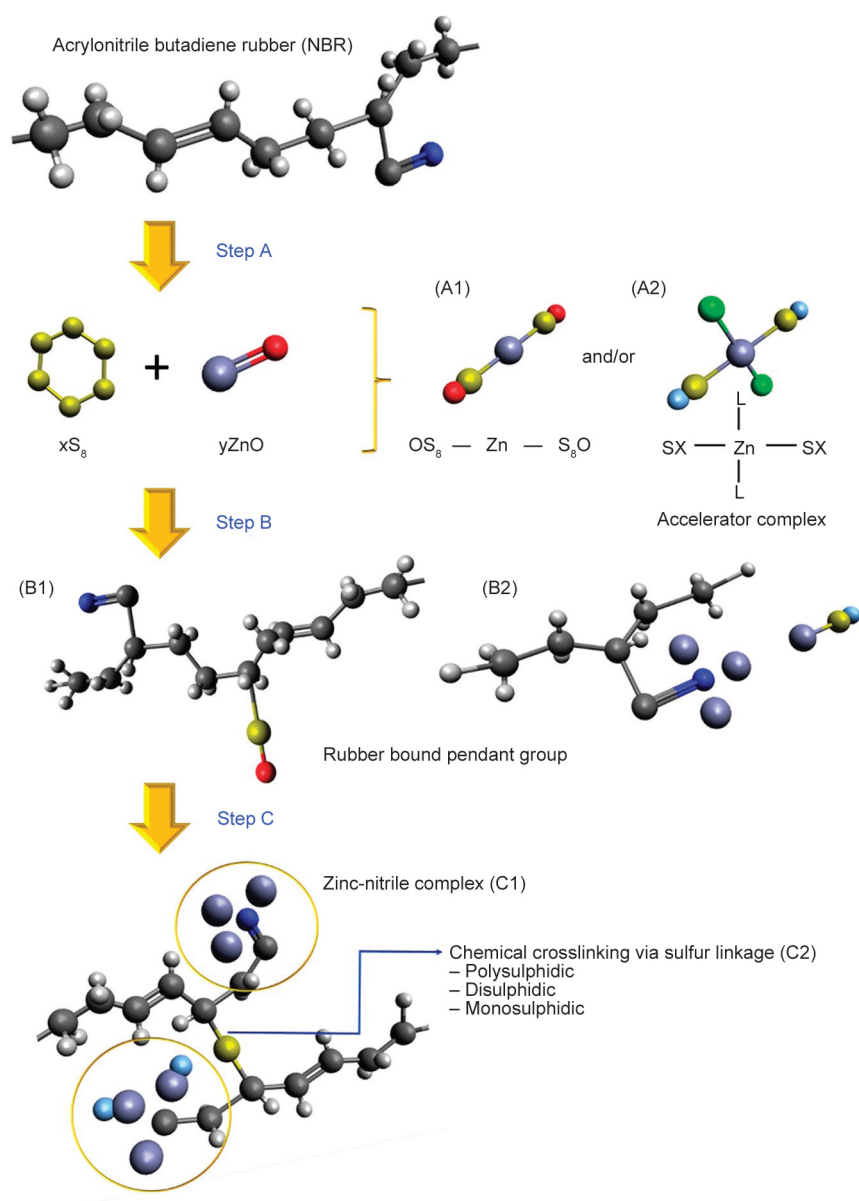


Figure 6. Proposed mechanism of chemical crosslinking and Zn ions interaction inside the NBR films filled with ZnO and sulfur. Here, the black, gray, blue, purple, yellow, red, green and light blue atoms refer to carbon, hydrogen, nitrogen, zinc, sulfur, oxygen, ligand and X atoms, respectively.

in the reaction with the nitrile group of NBR to form a zinc-nitrile complex. As a ligand, this donates the electron pair to the zinc present in the complex structure and accelerates the entire process [23]. Therefore, in Step C, the (B2) is still existed as the (C2), while the (B1) can propagate into (C1), relating the formation of sulfur bonding among the NBR molecules by means of poly-, di- and mono-sulphidic crosslinks [22, 23].

4.2.2. Mooney-Rivlin model

The reinforcement efficiency of each ZnO type regarding the NBR composite film matrix can be explained by the arrangement of the NBR molecular chains during extension by fitting the Mooney–Rivlin model to the stress–strain data in Figure 3 using Equation (3) [24]:

$$\sigma^*(\lambda) = \frac{\sigma(\lambda)}{\lambda - \lambda^{-2}} = 2(C_1 + C_2\lambda^{-1}) \quad (3)$$

where $\sigma^*(\lambda)$ is the reduced engineering stress; $\sigma(\lambda)$ is the engineering stress; and C_1 and C_2 are the characteristic constants of network chains, determined from the intercept and the slope of the curves, respectively. The extension ratio, λ , is given by $\lambda = 1 + \varepsilon$, where ε is the engineering strain. Based on the relationship of the calculated reduced stress, $\sigma^*(\lambda)$, as a function of the inverse of the extension ratio

($1/\lambda$), the chemical interactions of the films – the chemical crosslinking among the NBR molecular chains [25, 26] – are represented in Figure 7a, as compared to the physical interactions in Figure 7b. The obtained C_1 values are related to the y-intercept of the linear fit to the plot of $\sigma^*(\lambda)$ versus $1/\lambda$, and C_2 , determined from the slope of the fit, is related to the physical interactions (molecular chain entanglement and physical absorption). From the incorporation of the investigated ZnO types, the C_2 values were higher than those of C_1 . This clarifies that most of the NBR molecules have good interactions with the filler surface through physical chain entanglement based on their intermolecular chain attraction. The C_2 value increases upon the addition of 4 phr of $\text{ZnO}_{\text{nap-C}}$, which correlates well with the increased 100% modulus and tensile strength of the film. This implies that the proper addition of $\text{ZnO}_{\text{nap-C}}$ leads to better dispersion within the film and enhances the degree of reinforcement provided by the filler to the rubber matrix. In addition, considering the C_1 , it is clearly seen that the NBR/ $\text{ZnO}_{\text{nap-C}}$ showed the highest chemical interaction inside the films relative to others. It affirms the role of Zn ions releasing from the ZnO particles relating to the chemical crosslinking mechanism proposed in Figure 6. This strong crosslinking among the NBR molecules results in the formation of smooth surfaces on the NBR film, as

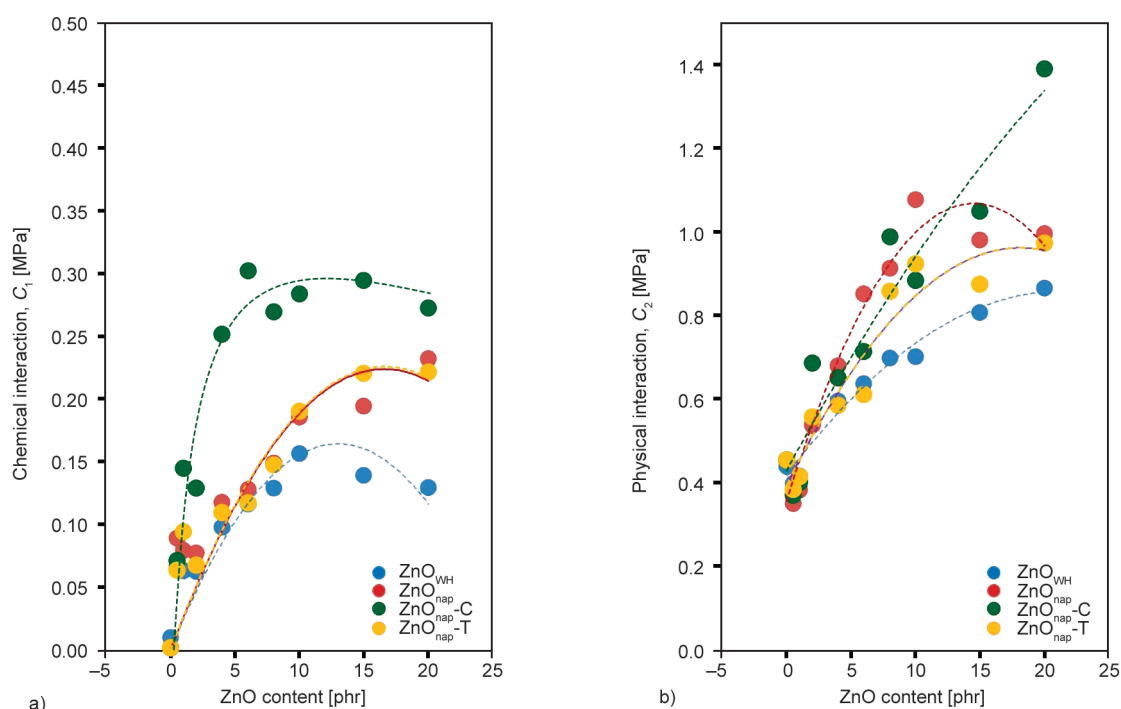


Figure 7. Chemical interaction (a) and physical interaction (b) of the NBR composite films filled with commercial ZnO_{WH} together with unmodified and modified ZnO_{nap} , calculated through the Mooney-Rivlin equation.

illustrated in the OM images presented in Figure 8. The smoothest surface is observed in the NBR com-

posite films filled with $\text{ZnO}_{\text{nap}}\text{-C}$, while the other composites exhibit significant filler agglomeration

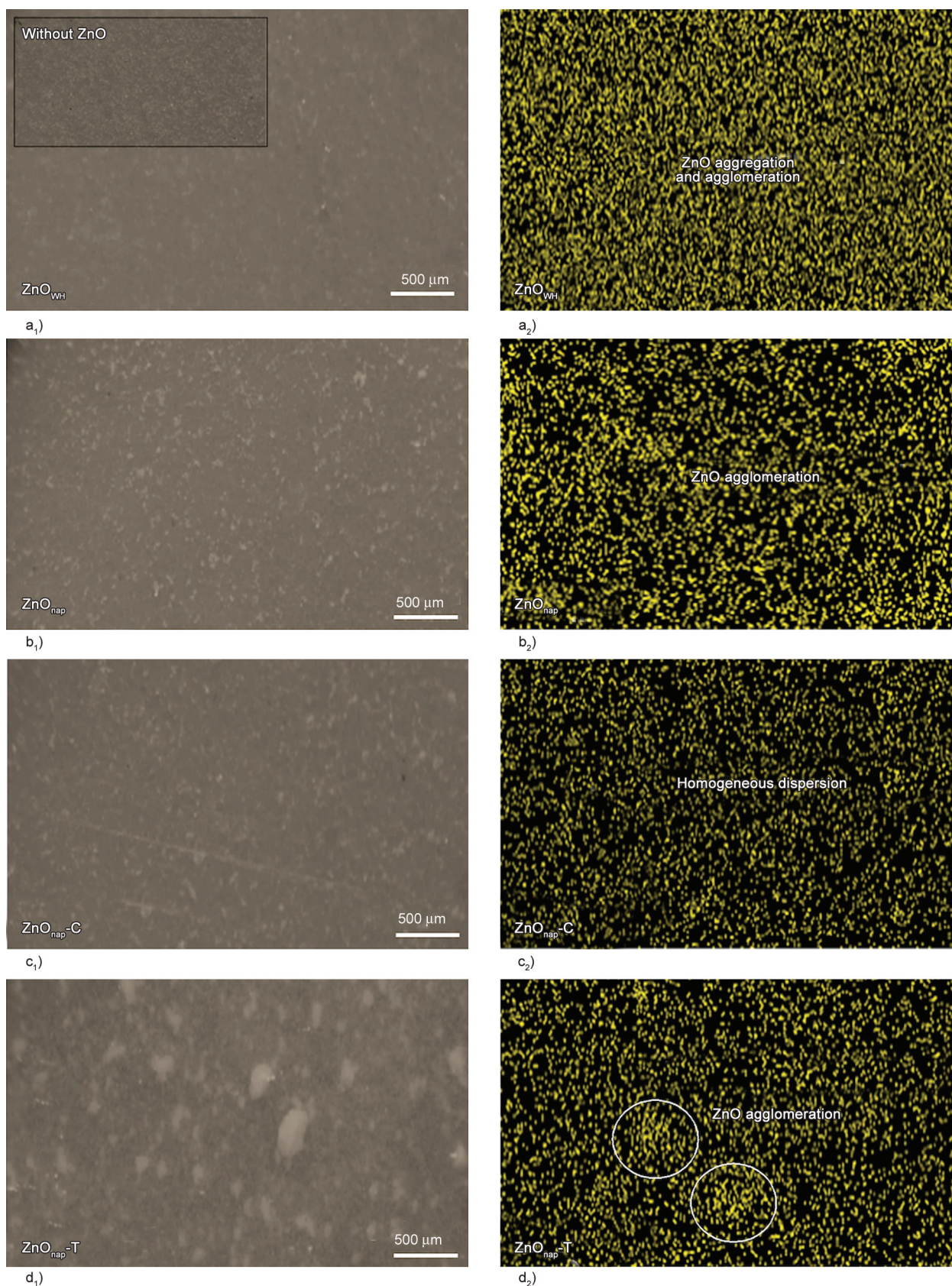


Figure 8. Morphologies observed of the OM of the NBR composites films filled with commercial ZnO_{WH} together with unmodified and modified ZnO_{nap} . a₁), a₂) ZnO_{WH} , b₁), b₂) ZnO_{nap} , c₁), c₂) $\text{ZnO}_{\text{nap}}\text{-C}$, d₁), d₂) $\text{ZnO}_{\text{nap}}\text{-T}$.

and rougher surfaces. The SEM-EDX images demonstrate the agglomeration of ZnO, ZnO_{nap}, and modified ZnO_{nap}, highlighting the effective dispersion and distribution of ZnO_{nap}-C within the NBR matrix, as depicted in Figure 8.

4.2.3. Dynamic mechanical analysis

Not only the mechanical but also the dynamic mechanical properties of the NBR films need to be determined with regard to the elasticity at different temperatures. Figure 9 plots the storage modulus (ϵ') and loss tangent ($\tan \delta$) as a function of temperature, which ranges from -80 to 100 °C. In addition, Table 3 summarizes the glass transition temperature (T_g) and $\tan \delta$ in terms of the maximum value ($\tan \delta_{\max}$) and the values at 0 °C ($\tan \delta_0$) and 60 °C ($\tan \delta_{60}$). The highest value of ϵ' was obtained for the pure NBR, which shows a slightly higher ϵ' than the NBR films filled with ZnO_{nap}-C and ZnO_{nap}. This might be due to the strong chain entanglement of the polar NBR chains, which effectively retards the physical chain deformation at low strain levels. This reasonably leads to obtaining the lowest T_g and highest $\tan \delta_{\max}$ for the unfilled NBR film, with both values referring to the elasticity of the film. The NBR/ZnO_{nap}-C composite shows the lowest T_g and highest $\tan \delta_{\max}$ values from among the filled NBR composites since it contains the highest crosslink density. The temperature that needs to be applied for the film to transition from a glassy to a rubbery state is, therefore, very low, and ϵ' changes significantly, leading to a high

$\tan \delta_{\max}$. On the other hand, the NBR films filled with ZnO_{nap} and ZnO_{nap}-T show increased T_g and decreased $\tan \delta_{\max}$ values relative to those of the NBR/ZnO_{nap}-C composite, with the NBR/ZnO_{WH} film yielding a considerably higher T_g value, significantly above 0 °C, and the lowest $\tan \delta_{\max}$. This implies that the addition of modified ZnO_{nap}, in particular, ZnO_{nap}-C, improves the elasticity of the NBR film to a greater extent than the other ZnO types by imparting a superior crosslink density and enhanced mechanical properties to the film.

The performance of the NBR films over the investigated temperature range can be interpreted through the $\tan \delta$ values at 0 and 60 °C. One can note that a lower $\tan \delta_{60}$ value is needed, relating to the requirement of high elasticity when handling the films in high-temperature conditions. In contrast, a higher $\tan \delta_0$ is required due to the hardening of the films in low-temperature conditions. Table 3 shows that NBR/ZnO_{nap}-C yields the lowest $\tan \delta_{60}$, which is related to the chemical crosslink density and elasticity

Table 3. Glass transition temperature (T_g) and Tan delta ($\tan \delta$) of NBR composite films filled with different types ZnO at 4 phr.

ZnO types	T_g [°C]	$\tan \delta_{\max}$	$\tan \delta$ at 0 °C	$\tan \delta$ at 60 °C
NBR	-8.50	0.726	0.582	0.188
NBR/ZnO _{WH}	3.33	0.300	0.297	0.215
NBR/ ZnO _{nap}	-4.33	0.357	0.335	0.087
NBR/ ZnO _{nap} -C	-5.83	0.497	0.448	0.078
NBR/ ZnO _{nap} -T	-2.67	0.302	0.298	0.152

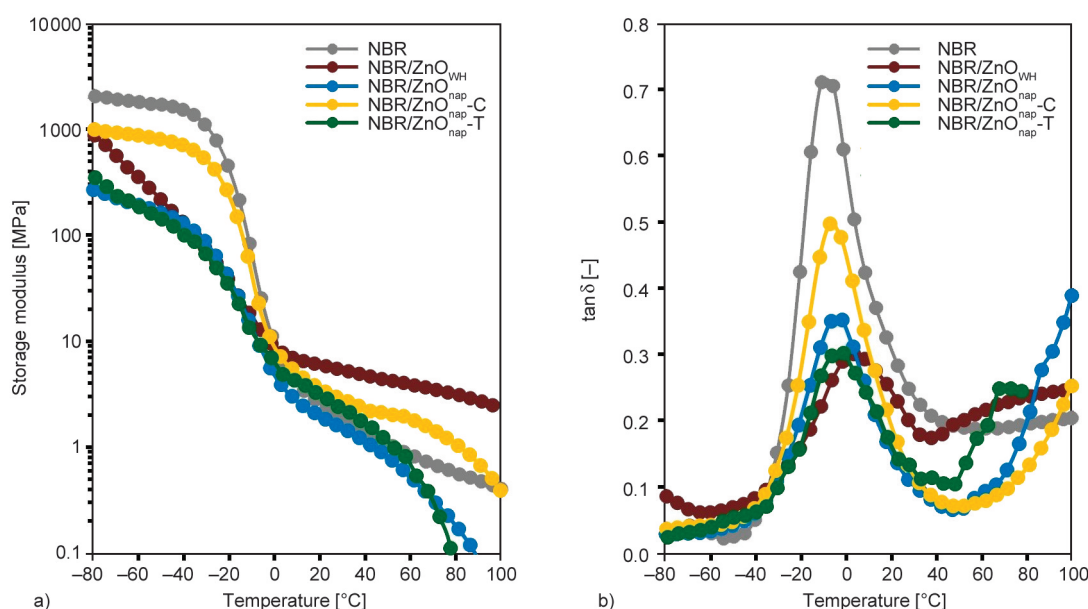


Figure 9. Storage modulus (a) and $\tan \delta$ (b) of NBR composites films filled with commercial ZnO_{WH} together with unmodified and modified ZnO_{nap} at 4 phr.

of the films. On the other hand, the NBR/ZnO_{WH} composite yields the highest $\tan \delta_{60}$ value due to its significantly high T_g and low ZnO_{WH} surface area for reacting with the film during crosslink propagation. In addition, it was observed that the NBR/ZnO_{WH} composite exhibited the highest value of ϵ' at temperatures above approximately 30 °C. This indicates that the elasticity effectively decreased beyond room temperature under dynamically low strain. This phenomenon could be attributed to the embedding of rubber molecules within aggregate and agglomerate structures, known as occluded rubber. The presence of numerous particulate aggregations in Figure 8 suggests the existence of extensive areas of occluded rubber in the NBR/ZnO_{WH} composite, which helps counteract crosslinked rubber deformation during low-strain application [27, 28]. Regarding $\tan \delta_0$, although the pure NBR shows the highest value, its combination with ZnO_{nap}-C yields the highest value relative to the other film composites. Therefore, considering the tensile properties and elasticity of the films, the incorporation of ZnO_{nap}-C significantly improved the film properties due to the filler's large surface area and good dispersion within the NBR matrix.

4.2.4. Antibacterial properties of NBR composite films

The incorporation of modified ZnO into NBR composite films significantly impacted the films' mechanical and dynamic mechanical properties based on particle size, dispersion considerations and ability for generating chemical crosslinking inside the films. In addition, given that ZnO displays excellent antibacterial performance, the composite films filled with modified ZnO (ZnO_{nap}-C) were evaluated in comparison with those containing commercial ZnO (ZnO_{WH}) for their antibacterial activity through qualitative and quantitative measurements. The qualitative determination was carried out using the Zone of Inhibition test, and the bactericidal efficiency on the film surface was assessed according to the ISO 22196:2011 and ASTM D7907-14 methods. This antibacterial ability can be originated following the photocatalytic processes onto ZnO particles. The *S. aureus* (ATCC 6538P) and *E. coli* (ATCC 8739) strains, which have been recognized as hospital-associated infections, were studied as representatives of Gram-positive and Gram-negative bacteria, respectively [29]; Figure 10 displays the results of the

Zone of Inhibition tests conducted on the NBR composite films, and the observed diameters of the zones of inhibition (clear zones) are given in Table 4. The clear zones, where there is no growth of bacteria, are notably visible in testing the composite films against *S. aureus*. The composite film filled with ZnO_{nap}-C displays a larger inhibition zone than the one with ZnO_{WH}, as shown in Table 4. One can observe the formation of the clear zones after the addition of 2 phr ZnO_{WH} and ZnO_{nap}-C, as shown in Figure 10. In addition, one should note that ZnO loadings over 10 phr are impractical due to the flocculation of the ZnO particles during the process. On the other hand, clear zones in testing the composite films against *E. coli* are not observed, implying that the composite films might have a greater bacterial killing ability against *S. aureus* than *E. coli*.

The ISO 22196:2011 method was used to prove the presence of antibacterial activity on the film surface in direct contact with the bacteria. The colony-forming units were counted to evaluate the antibacterial activity of the NBR composites after 24 h of incubation and assess the bacterial reduction efficacy, as shown in Figure 11. The results indicate that the composite films are effective against both bacterial types, with a bacterial reduction efficacy of 99.9% at a loading of at least 1 phr for ZnO_{nap}-C and above 2 phr for ZnO_{WH}. Thus, these results demonstrate the antibacterial ability of composite films incorporating nano-sized ZnO particles with small sizes and high specific surface areas, which are more effective in inhibiting bacterial growth than equivalent amounts of conventional ZnO. ZnO is recognized as a semiconductor material that has sufficient band gap energy to absorb photons for producing radical active species. The presence of ZnO in NBR composite films produces ROS, such as hydroxyl ($\cdot\text{OH}$), superoxide ($\cdot\text{O}_2^-$), and peroxy ($\text{HOO}\cdot$) radicals and hydrogen peroxide (H_2O_2), which are released onto the ZnO surface via a photocatalytic process and play an important role in antibacterial mechanisms [30], as can be seen in the proposed model of Figure 12. In Figure 12a, upon exposure to light, electrons are excited from the valence to the conduction band, producing electron-hole pairs (e_{cb}^- , h_{vb}^+). The h_{vb}^+ is formed in the valence band and oxidizes water or moisture to form $\cdot\text{OH}$, while the e_{cb}^- in the conduction band reduces oxygen to produce $\cdot\text{O}_2^-$, which reacts further with H^+ to form $\text{HOO}\cdot$ and H_2O_2 and is finally reduced to $\cdot\text{OH}$. Among the ROS, $\cdot\text{OH}$ and

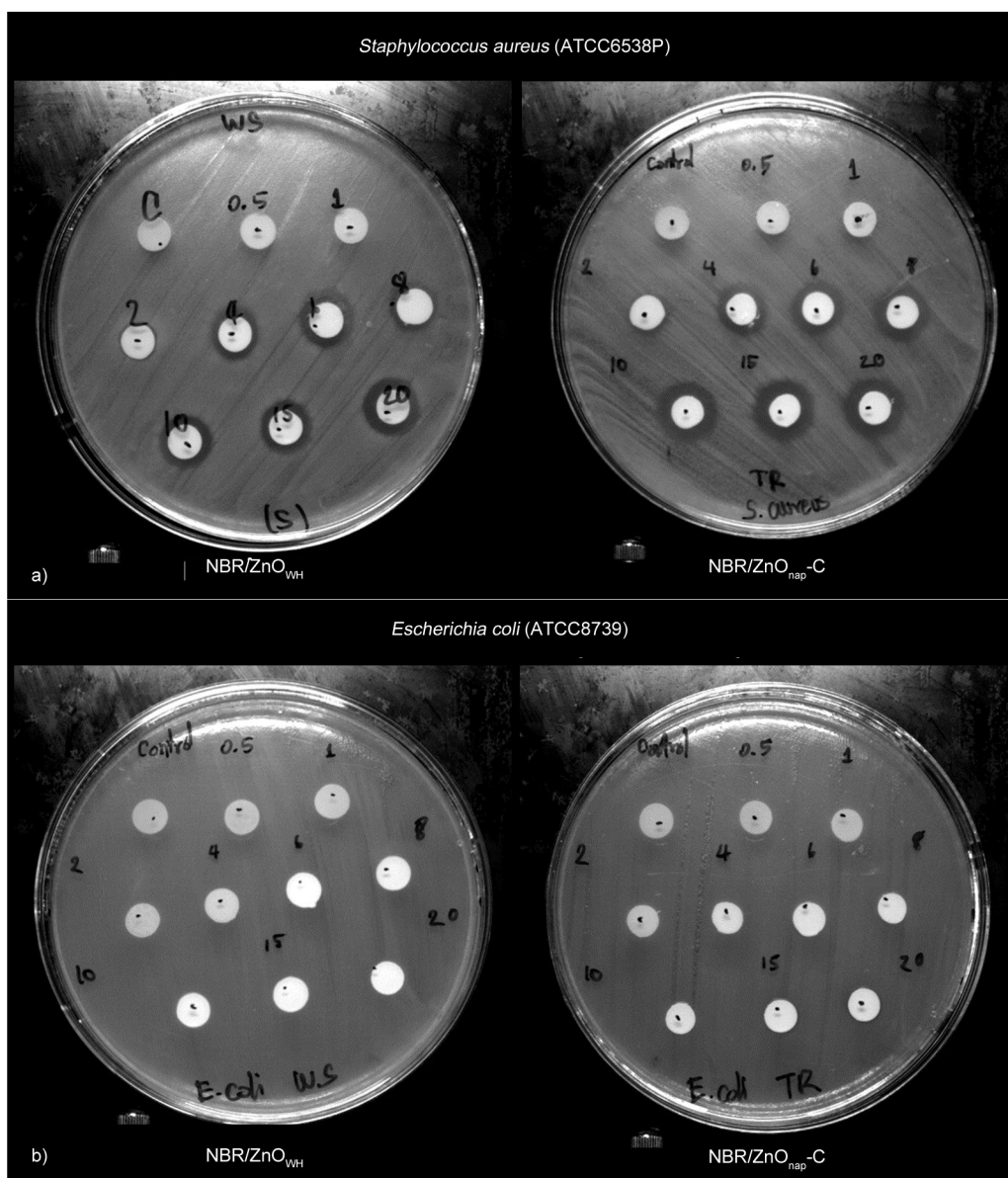


Figure 10. Agar disc diffusion of antibacterial against gram-positive *Staphylococcus aureus* (a) and gram-negative *Escherichia coli* (b) of NBR/ZnO_{WH} and NBR/ZnO_{nap-C} with varying ZnO loading at 0–20 phr.

Table 4. Diameter of inhibition clear zone of the NBR composite films filled with ZnO_{WH} and ZnO_{nap-C}.

ZnO loading [phr]	Inhibition clear zone [mm]			
	<i>Staphylococcus aureus</i>		<i>Escherichia coli</i>	
	NBR/ZnO _{WH}	NBR/ZnO _{nap-C}	NBR/ZnO _{WH}	NBR/ZnO _{nap-C}
0.0	0.00	0.00	0.00	0.00
0.5	0.00	0.00	0.00	0.00
1.0	0.00	0.00	0.00	0.00
2.0	1.08±0.57	0.70±0.71	0.00	0.00
4.0	3.64±0.48	3.15±0.72	0.00	0.00
6.0	4.10±0.76	3.75±0.62	0.00	0.00
8.0	3.12±0.55	4.43±0.47	0.00	0.00
10.0	4.56±0.44	5.76±0.36	0.00	0.00
15.0	4.48±0.41	5.59±0.80	0.00	0.00
20.0	5.25±0.87	5.77±0.56	0.00	0.00

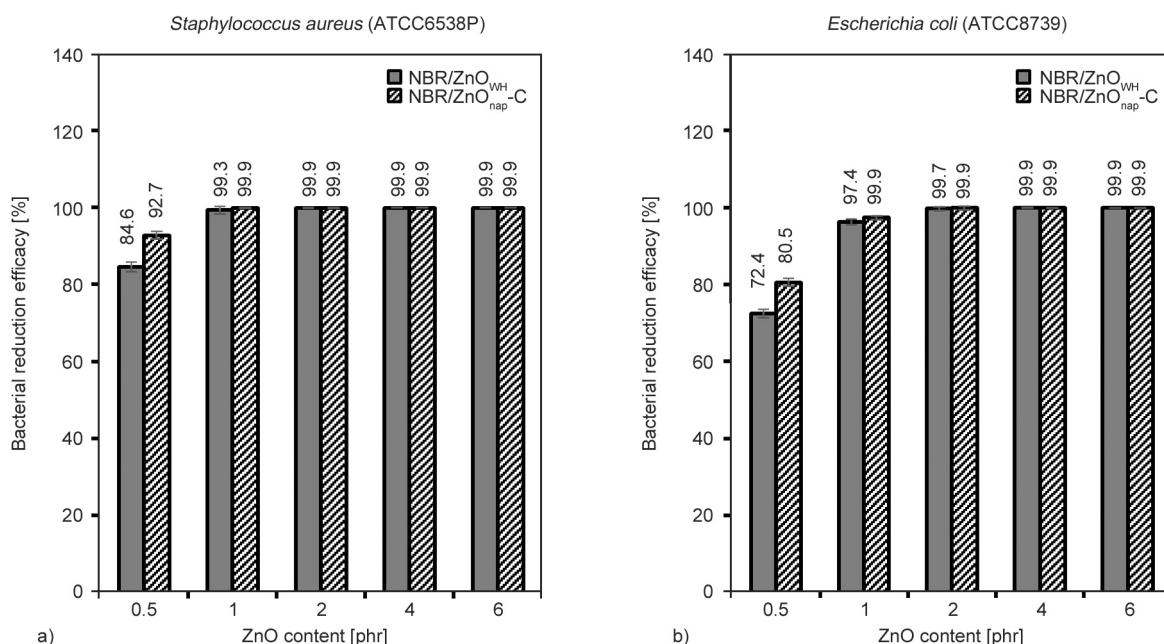


Figure 11. Bacterial reduction efficacy against Gram-positive *Staphylococcus aureus* (a) and Gram-negative *Escherichia coli* (b) of NBR films filled ZnO_{WH} and ZnO_{nap-C} with varying ZnO loading at 0.5–6.0 phr.

H₂O₂ are recognized as highly reactive species that play a crucial role in antibacterial activity by penetrating the outer membrane of cells, oxidizing the membrane lipids, enzymes, and proteins and causing deoxyribonucleic acid (DNA) damage [31–33]. Finally, intracellular components become damaged, leading to cell death. The release of Zn²⁺ ions through the rubber layer is another factor that plays a role in bacterial inactivation. The solubilized Zn²⁺ ions reach the outer cell wall and penetrate the cell membrane, reacting with the DNA within the bacterial cells by impeding transportation along with amino acid processing and by disrupting the enzyme system, which leads to bacterial cell death [33] (Figure 12c). In addition, the formation of ROS and the release of Zn²⁺ ions are influenced by the ZnO particle size. ZnO nanoparticles with smaller particle sizes and higher specific surface areas are more efficient in producing ROS and Zn²⁺ ions [30], which is related to Figure 2 and Table 2. The incorporation of ZnO_{nap-C} nanoparticles at 0.5 phr leads to a greater reduction in both bacterial types than the ZnO_{WH} microparticles. However, the release of both Zn²⁺ and ROS is also related to the ion's movement across the bound rubber to the film surfaces for attacking bacteria. In Figure 12b, it is seen that the ion attraction of zinc-nitrile complexes is the key potential factor for the movement of the existing ions. It is hypothesized that, after the photocatalytic processes, Zn²⁺ had connected closely to the ROS[−] which easily moved into NBR through ion-ion

intermolecular forces at the CN in the nitrile unit. This carried both ions to the films' surfaces and met with bacteria and microorganisms relatively.

The bactericidal efficacy on the surface of the NBR composite films against *S. aureus* and *E. coli*, with varying contact kill times of 0, 5, 10, 20, and 30 min, was determined according to the ASTM D7907-14 method, as shown in Figure 13. Bacterial reduction occurs after a contact time of 0 min, as measured by the number of colonies on the composite surface after dropping a bacterial suspension onto the material, covering it with a sterilized polyethylene film for 15 s, and subsequently removing it with a neutralizer solution. This indicates that an antibacterial reaction of ZnO is immediately triggered to kill microorganisms on the composite surface. The results after a contact time of 30 min reveal that the incorporation of ZnO_{nap-C} at 4 phr in the composite films leads to 92.00 and 51.85% bacterial reduction efficacy against *S. aureus* and *E. coli*, respectively. Furthermore, ZnO shows greater antibacterial activity against *S. aureus* than the *E. coli*, bacterium, as shown in Figure 13, respectively, due to differences in the structure, chemical composition, and polarity of the bacterial cell membranes. The Gram-negative *E. coli* has a larger negative charge than the Gram-positive *S. aureus* because of its additional lipopolysaccharide layer with a negative potential [34], as depicted in Figure 14; this leads to a lower concentration of negatively charged free radicals, such as superoxide

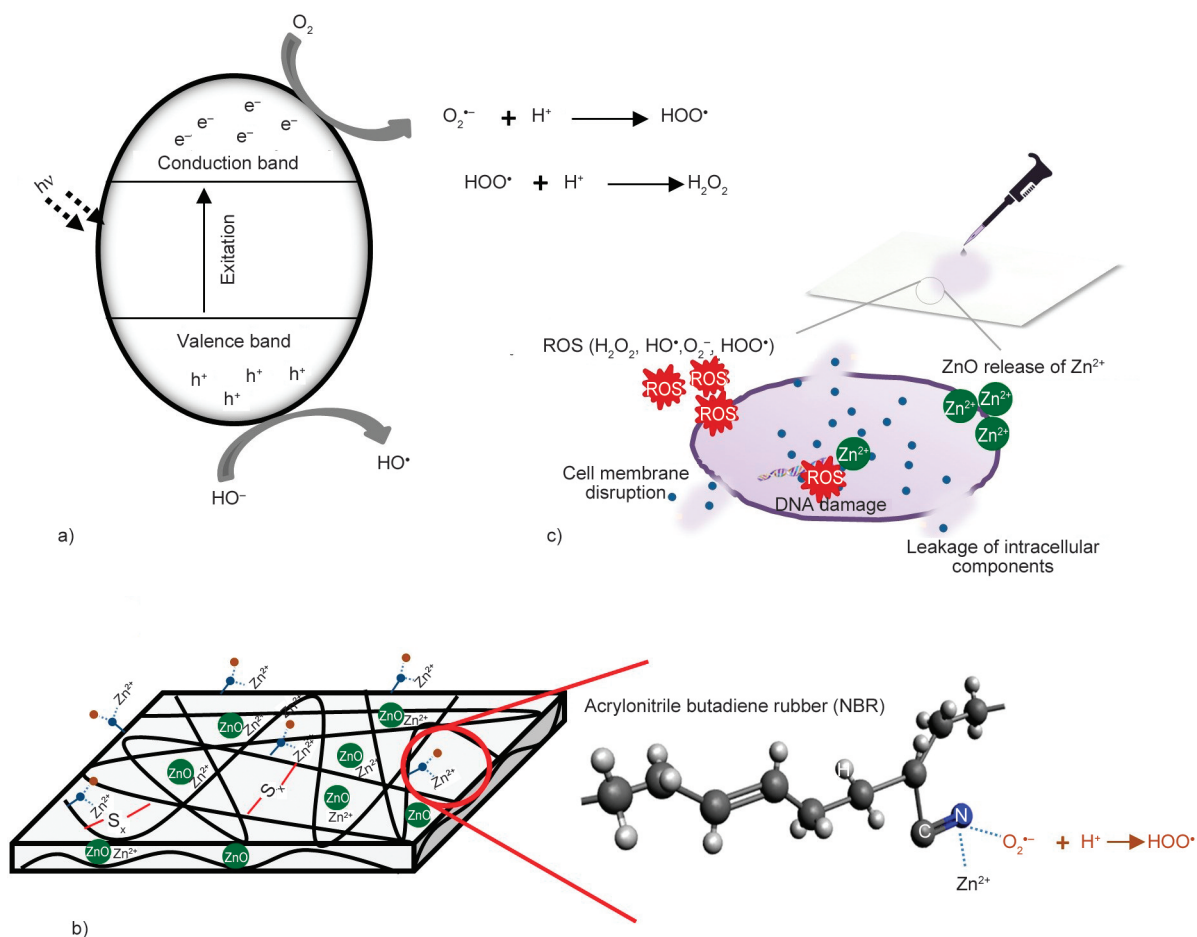


Figure 12. Proposed model of photocatalytic of ZnO particles (a), releasing mechanism for Zn^{2+} and ROS $^-$ to the NBR film surface (b) and bacteria disruption from Zn^{2+} and ROS (c).

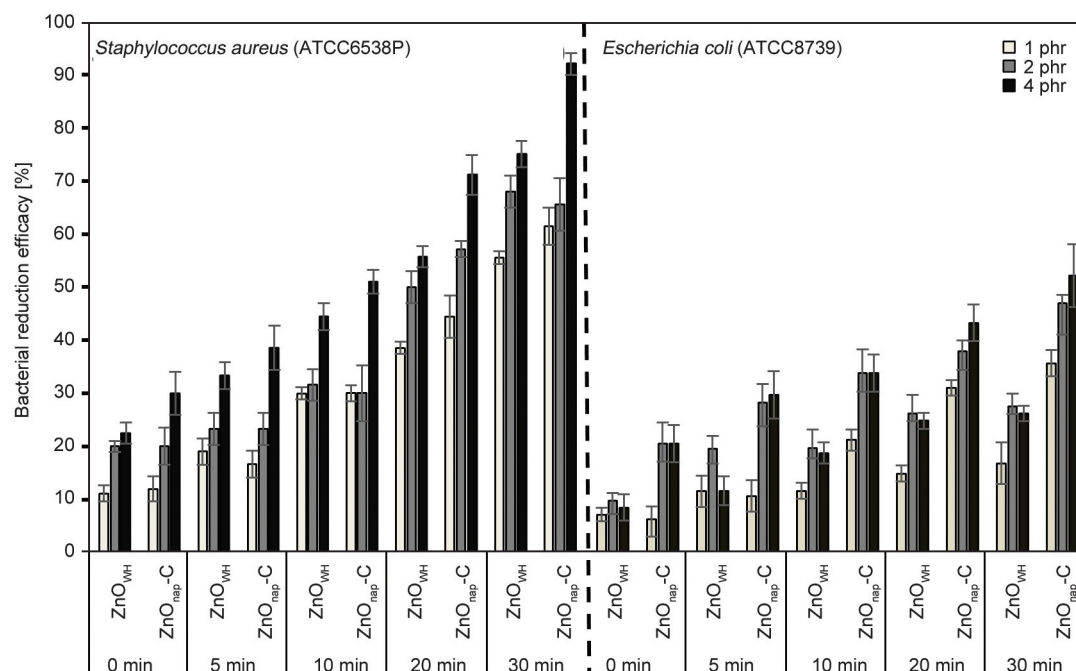


Figure 13. Bacterial reduction efficacy against gram-positive *Staphylococcus aureus* and gram-negative *Escherichia coli* of NBR films filled ZnO_{WH} and ZnO_{nap-C} with varying contact time.

anions, and peroxide ions penetrating the *E. coli* bacterial cell wall. In addition, *E. coli* has two cell membranes, including inner and outer ones, as shown in Figure 14, while *S. aureus* has one. The outer membrane of Gram-negative bacteria is covered with lipopolysaccharides, which act as a permeability barrier and protect the cells from potentially harmful agents [35]. In comparing the ZnO types, ZnO_{nap}-C exhibits a higher percentage of bacterial reduction than ZnO_{WH} due to its larger surface area, which leads to a large production of ROS and Zn²⁺ ions to damage bacterial cells. In addition, when evaluating the bacterial reduction efficiencies at different concentrations and contact times between rubber and bacteria using ZnO_{nap}, a 99.9% reduction was achieved at a ZnO_{nap} concentration of 2 phr for both *S. aureus* and *E. coli*. In addition, at a ZnO_{nap} concentration of 4 phr, a reduction of 75.5±3.5% for *S. aureus* and 51.0±7.5% for *E. coli* was observed, surpassing the efficiencies of ZnO_{WH} and showing slight variation compared to ZnO_{nap}-C. This finding aligns with the recent study by Krainoi *et al.* [18], where ZnO_{nap} exhibited lower antibacterial efficiency than modified ZnO_{nap} due to differences in dispersion and distribution within the rubber matrix. However, while ZnO_{nap} demonstrated high bacteria-killing performance, its purity was found to be

equivalent to that of ZnO_{WH} at 99.9%, whereas ZnO_{nap}-C exhibited a purity of only 90%. This result indicates that nanoparticles present the advantage of possibly reducing the amount of modified ZnO, especially ZnO_{nap}-C, in NBR composites while still significantly improving their mechanical and dynamic mechanical properties and antibacterial activity. Therefore, using modified ZnO nanoparticles in NBR composite films presents a good alternative to applying medical disinfection products to prevent the spread of pathogens.

5. Conclusions

NBR composite films incorporating different ZnO types, including white seal ZnO (ZnO_{WH}), ZnO nanoparticles (ZnO_{nap}), CaCO₃-coated ZnO_{nap} (ZnO_{nap}-C), and TiO₂-coated ZnO_{nap} (ZnO_{nap}-T), were investigated via a latex processing technique. Based on the characteristic structures of the ZnO types, the variations in particle size, band gap energy, and Zn²⁺ ion solubility affect the properties of the composite films. The mechanical and dynamic mechanical properties, crosslink density, and antibacterial activity of the composite films were considered; the results indicated that the ZnO particle size and distribution play an important role in improving the crosslink density and mechanical characteristics. The composite

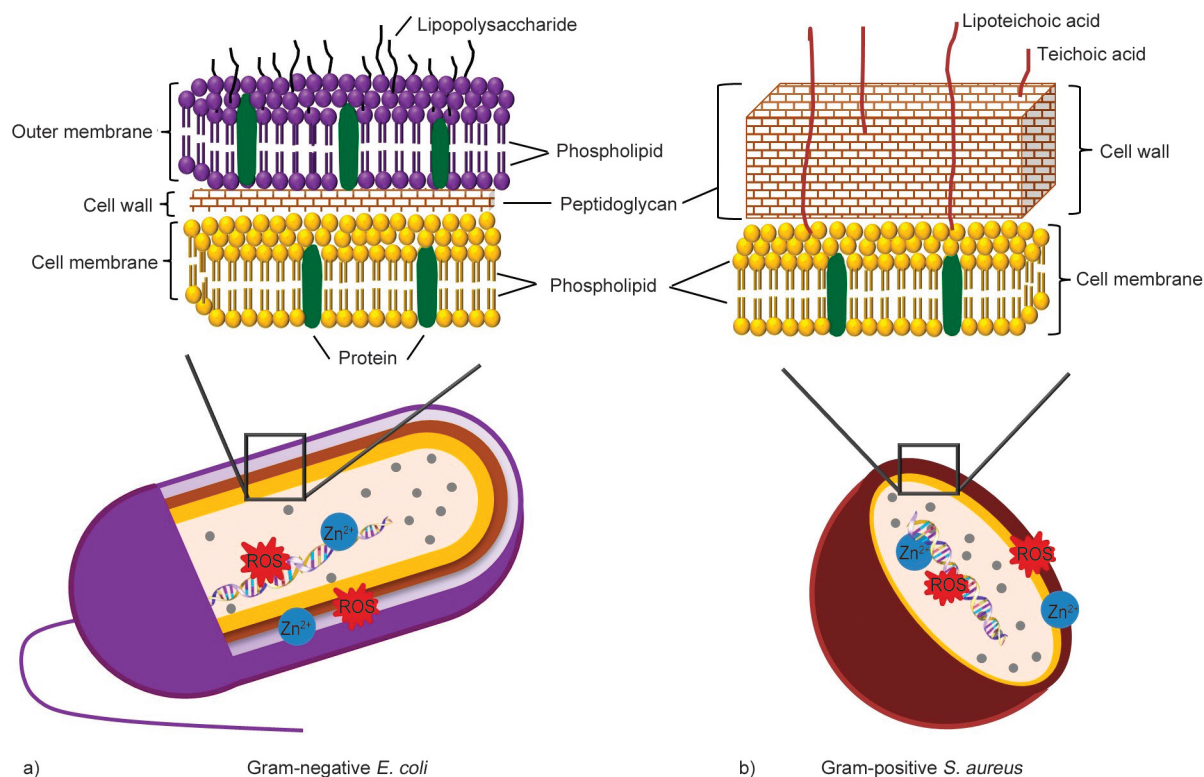


Figure 14. Proposed model of antibacterial mechanisms of ZnO to Gram-negative *E. coli* (a) and Gram-positive *S. aureus* (b).

filled with ZnO_{nap}-C activated chemical crosslinking, which was in good agreement with the increased tensile modulus, Mooney–Rivlin plot, and dynamic mechanical results for this composite. In contrast, the incorporation of ZnO_{nap} and ZnO_{nap}-T gave rise to less enhanced properties in the composites due to the presence of significant ZnO agglomeration. In addition, the low specific surface area of the ZnO_{WH} microparticles in their reaction with the NBR molecules during crosslinking led to the least favorable composite properties. The antibacterial activity of the composite films was evaluated through qualitative and quantitative determinations using *S. aureus* and *E. coli* as representatives of hospital-associated infections. The results indicated that both the NBR composite films with ZnO_{WH} and ZnO_{nap}-C exhibit an inhibition zone against *S. aureus*, while no such observation was made for *E. coli*. However, antibacterial activity on the composite film surface in direct contact with the bacterial cells, tested according to ISO 22196:2011, was observed against both bacterial types, with 99.9% bacterial reduction efficacy at loadings of 1 phr for ZnO_{nap}-C and over 2 phr for ZnO_{WH}. Bacterial cell structure disruption was achieved through the formation of ROS radicals and the release of Zn²⁺ ions, which can be related to the obtained band gap energy and partial solubility of ZnO to release Zn²⁺. In addition, in accordance with ASTM D7907-14, the bactericidal efficacy on the composite film surfaces at various contact kill times between 0 and 30 min was determined. The addition of ZnO_{nap}-C at 4 phr yielded 92.00 and 51.85% bacterial reduction efficacy within 30 min against *S. aureus* and *E. coli*, respectively. The results suggest that the use of nanoparticles could reduce the amount of modified ZnO, particularly ZnO_{nap}-C, in NBR composites, which is in good agreement with the measured mechanical, dynamic mechanical, and antibacterial properties of the composites. To prevent the spread of pathogens, the use of modified ZnO nanoparticles in NBR composite films in, for example, gloves and multipurpose rubber films presents a suitable alternative to using medical disinfection products.

Acknowledgements

The authors gratefully acknowledge the Thailand Science Research and Innovation (TSRI) Basic Research Fund: The fiscal year 2023 under project number FRB660073/0164 was acknowledged.

References

- [1] Critchley E., Pemberton M. N.: Latex and synthetic rubber glove usage in UK general dental practice: Changing trends. *Heliyon*, **6**, e03889 (2020).
<https://doi.org/10.1016/j.heliyon.2020.e03889>
- [2] Bodilsen J., Brouwer M. C., Kjærgaard N., Sirks M. J., van der Ende A., Nielsen H., van de Beek D.: Community-acquired meningitis in adults caused by *Escherichia coli* in Denmark and The Netherlands. *Journal of Infection*, **77**, 25–29 (2018).
<https://doi.org/10.1016/j.jinf.2018.05.009>
- [3] Tian L., Sun Z., Zhang Z.: Antimicrobial resistance of pathogens causing nosocomial bloodstream infection in Hubei province, China, from 2014 to 2016: A multicenter retrospective study. *BMC Public Health*, **18**, 1121 (2018).
<https://doi.org/10.1186/s12889-018-6013-5>
- [4] Čustović A., Smajlović J., Hadžić S., Ahmetagić S., Tihic N., Hadzagić H.: Epidemiological surveillance of bacterial nosocomial infections in the surgical intensive care unit. *Materia Socio-Medica*, **26**, 7–11 (2014).
<https://doi.org/10.5455/msm.2014.26.7-11>
- [5] Sari N. M., Gwee K., Maher S., Rashid A. A.: Natural rubber (NR) latex films with antimicrobial properties for stethoscope diaphragm covers. *Materials*, **15**, 3433 (2022).
<https://doi.org/10.3390/ma15103433>
- [6] Koedrit P., Thasiphu T., Jong W-I., Boonprasert R., Tuitemwong K., Tuitemwong P.: Recent trends in rapid environmental monitoring of pathogens and toxicants: Potential of nanoparticle-based biosensor and applications. *Nanomaterials and Nanodevices*, **2015**, 510982 (2015).
<https://doi.org/10.1155/2015/510982>
- [7] Ishida T.: Antibacterial mechanism of Ag⁺ ions for bacteriolyses of bacterial cell walls *via* peptidoglycan autolysins, and DNA damages. *MOJ Toxicology*, **4**, 345–350 (2018).
<https://doi.org/10.15406/mojt.2018.04.00125>
- [8] Salah I., Parkin I. P., Allan E.: Copper as an antimicrobial agent: Recent advances. *RSC Advances*, **11**, 18179–18186 (2021).
<https://doi.org/10.1039/D1RA02149D>
- [9] Sirelkhatim A., Mahmud S., Seeni A., Kaus N. H., Ann L. C., Bakhori S. K., Hasan H., Mohamad D.: Review on zinc oxide nanoparticles: Antibacterial activity and toxicity mechanism. *Nano-Micro Letters*, **7**, 219–242 (2015).
<https://doi.org/10.1007/s40820-015-0040-x>
- [10] Kubacka A., Diez M. S., Rojo D., Bargiela R., Ciordia S., Zapico I., Albar J. P., Barbas C., dos Santos V. A. P. M., Fernández-García M., Ferrer M.: Understanding the antimicrobial mechanism of TiO₂-based nanocomposite films in a pathogenic bacterium. *Scientific Reports*, **4**, 4134 (2014).
<https://doi.org/10.1038/srep04134>

- [11] Mendes C. R., Dilarri G., Forsan C. F., de Moraes Ruy Sapata V., Lopes P. R. M., de Moraes P. B., Montagnoli R. N., Ferreira H., Bidoia E. D.: Antibacterial action and target mechanisms of zinc oxide nanoparticles against bacterial pathogens. *Scientific Reports*, **12**, 2658 (2022). <https://doi.org/10.1038/s41598-022-06657-y>
- [12] Rutherford D., Jira J., Kolářová K., Matolínová I., Mičová J., Remeš Z., Rezek B.: Growth inhibition of gram-positive and gram-negative bacteria by zinc oxide hedgehog particles. *International Journal of Nanomedicine*, **16**, 3541–3554 (2021). <https://doi.org/10.2147/IJN.S300428>
- [13] Raj N. B., Pavithra Gowda N. P., Pooja O. S., Purushotham B., Kumar M. R. A., Sukrutha S. K., Ravikumar C. R., Nagaswarupa H. P., Murthy H. C. A., Boppana S. B.: Harnessing ZnO nanoparticles for antimicrobial and photocatalytic activities. *Journal of Photochemistry and Photobiology*, **6**, 100021 (2021). <https://doi.org/10.1016/j.jpap.2021.100021>
- [14] Zabrieski Z., Morrell E., Hortin J., Dimkpa C., McLean J., Britt D., Anderson A.: Pesticidal activity of metal oxide nanoparticles on plant pathogenic isolates of pythium. *Ecotoxicology*, **24**, 1305–1314 (2015). <https://doi.org/10.1007/s10646-015-1505-x>
- [15] Anwar M. A., Aqib A. I., Ashfaq K., Deeba F., Khan M. K., Khan S. R., Muzammil I., Shoaib M., Naseer M. A., Riaz T., Tanveer Q., Sadiq M., Lodhi F. L., Ashraf F.: Antimicrobial resistance modulation of MDR *E. coli* by antibiotic coated ZnO nanoparticles. *Microbial Pathogenesis*, **148**, 104450 (2020). <https://doi.org/10.1016/j.micpath.2020.104450>
- [16] El-Megharbel S. M., Alsawat M., Al-Salmi F. A., Hamza R. Z.: Utilizing of (zinc oxide nano-spray) for disinfection against 'SARS-CoV-2' and testing its biological effectiveness on some biochemical parameters during (COVID-19 Pandemic)-'ZnO nanoparticles have antiviral activity against (SARS-CoV-2)'. *Coatings*, **11**, 388 (2021). <https://doi.org/10.3390/coatings11040388>
- [17] Choi S.-S., Kim J.-C., Woo C.-S.: Accelerated thermal aging behaviors of EPDM and NBR vulcanizates. *Bulletin of the Korean Chemical Society*, **27**, 936–938 (2006). <https://doi.org/10.5012/bkcs.2006.27.6.936>
- [18] Krainoi A., Poomputsa K., Kalkornsrapranee E., Johns J., Songtipya L., Nip R., Nakaramontri Y.: Disinfectant natural rubber films filled with modified zinc oxide nanoparticles: Synergetic effect of mechanical and antibacterial properties. *Express Polymer Letters*, **15**, 1081–1100 (2021). <https://doi.org/10.3144/expresspolymlett.2021.87>
- [19] El-Nemr K. F., Radi H., Mousa I. M.: Properties of acrylonitrile butadiene rubber modified with acrylate monomers and oligomers using gamma irradiation. *Egyptian Journal of Radiation Sciences and Applications*, **30**, 145–152 (2017). <https://doi.org/10.21608/ejrsa.2018.1749.1019>
- [20] Deng X., Luan Q., Chen W., Wang Y., Wu M., Zhang H., Jiao Z.: Nanosized zinc oxide particles induce neural stem cell apoptosis. *Nanotechnology*, **20**, 115101 (2009). <https://doi.org/10.1088/0957-4484/20/11/115101>
- [21] Brüning K., Schneider K., Roth S. V., Heinrich G.: Kinetics of strain-induced crystallization in natural rubber studied by WAXD: Dynamic and impact tensile experiments. *Macromolecules*, **45**, 7914–7919 (2012). <https://doi.org/10.1021/ma3011476>
- [22] Passador F. R., Rodolfo A., Pessan L. A.: *In situ* dynamic vulcanization of poly(vinyl chloride)/acrylonitrile-butadiene rubber blends. *Journal of Macromolecular Science: Part B*, **48**, 282–298 (2009). <https://doi.org/10.1080/00222340802679607>
- [23] Hait S., Valentín J. L., Jimenez A. G., Ortega R., Ghosh A. K., Stöckelhuber K. W., Wießner S., Heinrich G., Das A.: Poly(acrylonitrile-*co*-butadiene) as polymeric cross-linking accelerator for sulphur network formation. *Heliyon*, **6**, e04659 (2020). <https://doi.org/10.1016/j.heliyon.2020.e04659>
- [24] Rivlin R. S., Saunders D. W.: Large elastic deformations of isotropic materials VII. Experiments on the deformation of rubber. *Philosophical Transactions of the Royal Society*, **243**, 251–288 (1951). <https://doi.org/10.1098/rsta.1951.0004>
- [25] Schlögl S., Trutschel M.-L., Chassé W., Riess G., Saalwächter K.: Entanglement effects in elastomers: Macroscopic vs microscopic properties. *Macromolecules*, **47**, 2759–2773 (2014). <https://doi.org/10.1021/ma4026064>
- [26] Saleesung T., Reichert D., Saalwächter K., Sirisinha C.: Correlation of crosslink densities using solid state NMR and conventional techniques in peroxide-crosslinked EPDM rubber. *Polymer*, **56**, 309–317 (2015). <https://doi.org/10.1016/j.polymer.2014.10.057>
- [27] Fröhlich J., Niedermeier W., Luginsland H.-D.: The effect of filler–filler and filler–elastomer interaction on rubber reinforcement. *Composites Part A: Applied Science and Manufacturing*, **36**, 449–460 (2005). <https://doi.org/10.1016/j.compositesa.2004.10.004>
- [28] Omnès B., Thuillier S., Pilvin P., Grohens Y., Gillet S.: Effective properties of carbon black filled natural rubber: Experiments and modeling. *Composites Part A: Applied Science and Manufacturing*, **39**, 1141–1149 (2008). <https://doi.org/10.1016/j.compositesa.2008.04.003>
- [29] Haque M., Sartelli M., McKimm J., Bakar M. A.: Health care-associated infections – An overview. *Infection and Drug Resistance*, **11**, 2321–2333 (2018). <https://doi.org/10.2147/idr.s177247>
- [30] Prasanna V. L., Vijayaraghavan R.: Insight into the mechanism of antibacterial activity of ZnO: Surface defects mediated reactive oxygen species even in the dark. *Langmuir*, **31**, 9155–9162 (2015). <https://doi.org/10.1021/acs.langmuir.5b02266>

- [31] Sawai J., Shoji S., Igarashi H., Hashimoto A., Kokugan T., Shimizu M., Kojima H.: Hydrogen peroxide as an antibacterial factor in zinc oxide powder slurry. *Journal of Fermentation and Bioengineering*, **86**, 521–522 (1998).
[https://doi.org/10.1016/S0922-338X\(98\)80165-7](https://doi.org/10.1016/S0922-338X(98)80165-7)
- [32] Bogdan J., Zarzyńska J., Pławińska-Czarnak J.: Comparison of infectious agents susceptibility to photocatalytic effects of nanosized titanium and zinc oxides: A practical approach. *Nanoscale Research Letters*, **10**, 309 (2015).
<https://doi.org/10.1186/s11671-015-1023-z>
- [33] Krishnamoorthy R., Athinarayanan J., Periyasamy V. S., Alshuniaber M. A., Alshammari G., Hakeem M. J., Ahmed M. A., Alshatwi A. A.: Antibacterial mechanisms of zinc oxide nanoparticle against bacterial food pathogens resistant to beta-lactam antibiotics. *Molecules*, **27**, 2489 (2022).
<https://doi.org/10.3390/molecules27082489>
- [34] Sonohara R., Muramatsu N., Ohshima H., Kondo T.: Difference in surface properties between *Escherichia coli* and *Staphylococcus aureus* as revealed by electrophoretic mobility measurements. *Biophysical Chemistry*, **55**, 273–277 (1995).
[https://doi.org/10.1016/0301-4622\(95\)00004-h](https://doi.org/10.1016/0301-4622(95)00004-h)
- [35] Li W-R., Xie X-B., Shi Q-Z., Zeng Y-N., Ou-Yang Y-S., Chen Y-B.: Antibacterial activity and mechanism of silver nanoparticles on *Escherichia coli*. *Applied Microbiology and Biotechnology*, **85**, 1115–1122 (2010).
<https://doi.org/10.1007/s00253-009-2159-5>